Vibration Reduction of Cable-Driven Parallel Robots through Elasto-dynamic Model-Based Control

Sana Baklouti, Eric Courteille, Philippe Lemoine, Stéphane Caro

Vibration Reduction of Cable-Driven Parallel Robots through Elasto-dynamic Model-Based Control

Sana Baklouti[a], Eric Courteille[a], Philippe Lemoine[c], Stéphane Caro[b,*]

[a] *Univ Rennes, INSA Rennes, LGCGM-EA 3913, F-35000 Rennes, France*
[b] *CNRS, LS2N, UMR CNRS 6004, Nantes, France*
[c] *Centrale Nantes, LS2N, UMR CNRS 6004, Nantes, France*

Abstract

This paper deals with the elasto-dynamic model-based control of Cable-Driven Parallel Robots (CDPRs), which manifests in the coupling of a PID feedback controller with a model-based feed-forward control scheme. The feed-forward controller is derived from an inverse elasto-dynamic model of CDPR, which compensates the end-effector dynamics and specifically its vibrations due to cable elasticity. The integration of cable tension calculation into this control strategy guarantees positive cable tensions along the trajectory. Simulations and experimentations while using a suspended and non-redundant CDPR show that tracking errors and vibrations can be reduced by the proposed strategy compared to conventional rigid-body model-based control.

Keywords: Cable-Driven Parallel Robot, Model-based control, Elasto-dynamic pre-compensation.

1. Introduction

Cable-Driven Parallel Robots (CDPRs) are a special kind of parallel robots, where rigid links are replaced by cables. A CDPR is decomposed into an end-effector (EE) connected to a fixed base frame through cables. CDPRs may be used in some application fields where industrial robots cannot be used due to limitation of their workspace, payload and the required cycle time. These specifications have attracted the interest of many researchers [1, 2, 3].

Thanks to their low inertia, CDPRs can reach high velocities and accelerations in large workspaces [4], which may lead to vibrations due to cable elasticity. Two main issues related to CDPRs are discussed: pose stabilization and trajectory tracking. While the pose stabilization aims to stabilize the robot in a reference pose, the trajectory tracking aims to have the EE following a reference trajectory.

*Corresponding author
Email addresses: Sana.baklouti@insa-rennes.fr (Sana Baklouti), Eric.courteille@insa-rennes.fr (Eric Courteille), Philippe.lemoine@ls2n.fr (Philippe Lemoine), Stephane.Caro@ls2n.fr (Stéphane Caro)

The improvement of the robot performance can be done through the modification of the robot architecture either by optimizing the design [5, 6, 7, 8] or by adding other components such as in [9, 10]. Improving accuracy is still possible once the robot is in operation through a suitable control scheme.

Several controllers have been proposed in the literature to improve CDPR accuracy locally or on trajectory tracking [11, 12, 13]. In [14], the control of CDPR in the operational space is presented while considering non elastic but sagging cables through the Assumed Mode Method. In [15], a discrete-time control strategy is proposed to estimate the position accuracy of the EE by taking into account the actuator model, the kinematic and static behavior of the CDPR.

Many papers deal with CDPR control while considering cable elongations and their effect on the dynamic behavior. A robust H_∞ control scheme for CDPR is described in [16] while considering the cable elongations into the dynamic model of the EE and cable tension limits. Assuming flexibility in the longitudinal direction of cable, a control strategy is proposed for CDPRs in [17], [18], [19]. It consists in adding an elongation compensation term in the control law of a CDPR with rigid cables, using singular perturbation theory to get rid of undesirable vibrations. Here, cables are modeled by linear axial springs, but with constant stiffness. This control method is improved in [20] by integrating variable cable stiffness. In this context, a robust adaptive controller is presented in [21] to attenuate vibrations in presence of kinematic and dynamic uncertainties. This control method requires the measurement of cable lengths and the knowledge of the real-time end-effector EE pose through exteroceptive measurements. However, the external-measurement-based control methods add complexity to the cable-driven manipulators and restrict the application conditions due to the need of additional devices [22].

The importance of the feed-forward effect on non-linear systems control is highlighted in [23]. It leads to stable systems with enhanced trajectory tracking performance. Feed-forward model-based controllers are used to fulfill accuracy improvement by using a CDPR reference model [24]. This latter predicts the mechanical behavior of the robot; and then generates an adequate reference signal to be followed by the CDPR. This control type leads to the compensation of the undesirable effects without exteroceptive measurements. A model-based control scheme for CDPR used as a high rack storage is presented in [25]. This research work takes into account cable elasticity. This strategy, integrating the mechanical behavior of cables in the reference signal, enhances the CDPR performance. However, the compensation for the EE pose errors due to the cable interaction with the whole system and elasto-dynamic behavior was not considered.

Consequently, we proposed an elasto-dynamic model-based control in [26] for only non-redundant CDPRs. This control method combines a model-based feed-forward control scheme for CDPRs with a PID feedback controller. The feed-forward controller is derived from an inverse elasto-dynamic model of CDPR, which compensates the EE deflection due to cable elasticity and vibrations due to dynamic interactions. The relevance of the proposed control method was checked

only numerically. Therefore, in addition of the work reported in [26], this paper gives more details on the improved control strategy and contains experimental validations of the obtained theoretical results. Moreover, this paper deals with the improvement of the elasto-dynamic model-based control strategy to make it valid for any CDPR configuration through the integration of cable tension distribution into this control strategy, guaranteeing positive cable tensions along the trajectory.

This paper is organized as follows: Section 2 presents the dynamic equations of motion of CDPR required to establish the control laws. Section 3 introduces the design of the elasto-dynamic model-based control and the definition of the corresponding control laws. Then, experimental validations performed on the CREATOR prototype located at LS2N, Nantes, France, a CDPR with three cables and three Degree-Of-Freedom (DOF), are discussed in detail in Section 4. Finally, the effectiveness of the proposed elasto-dynamic control strategy is studied numerically (Section 5) and experimentally (Section 6) to check its performance with regard to the CDPR positioning accuracy and trajectory tracking compared to the conventional ones.

2. Dynamic modeling of CDPR

The joint coordinate vector is denoted as $\mathbf{q} = [q_1,\ ...,\ q_n]^T \in \mathbb{R}^n$, n being the number of cables. As shown in Fig. 1, the Cartesian coordinate vectors of anchor points A_i and exit points B_i, $i = [1..n]$, are denoted as $\mathbf{a}_i$ and $\mathbf{b}_i$. These vectors are expressed in the EE frame $\mathcal{F}_p = \{P,\ x_p,\ y_p,\ z_p\}$ and in the base frame $\mathcal{F}_b = \{O,\ x_b,\ y_b,\ z_b\}$, respectively.

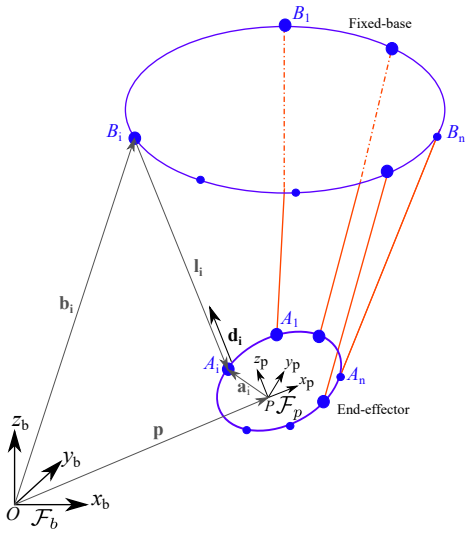

Figure 1: The ith closed-loop of a CDPR

The pose $\mathbf{x} = [\mathbf{p}^T \ \mathbf{o}^T]^T \in \mathbb{R}^m$ of the EE center P in the base frame $\mathcal{F}_b$ is described by the position vector $\mathbf{p} = [x,\ y,\ z]^T \in \mathbb{R}^u$ and the orientation vector $\mathbf{o} = [\phi,\ \theta,\ \psi]^T \in \mathbb{R}^v$. The orientation of the EE is parameterized by Euler angles ϕ, θ and ψ. u is the number of translational DOF, v is the number of rotational DOF and m is the total number DOF of the EE.

The ith cable connecting exit point B_i and anchor point A_i, $i = [1..n]$, exerts a force from A_i to B_i of magnitude τ_i>0. The ith cable length l_i is expressed as follows:

$$l_i = \|\mathbf{p} - \mathbf{b}_i + {}^b\mathbf{R}_p\mathbf{a}_i\|_2. \tag{1}$$

The relationship between the cable length vector $\mathbf{l} = [l_1,\ ...,\ l_n]^T \in \mathbb{R}^n$ and the motor angular displacement vector $\mathbf{q}$ is supposed to be linear:

$$\mathbf{l} = \boldsymbol{\chi}\ \mathbf{q}, \tag{2}$$

where $\boldsymbol{\chi} = \text{diag}[\chi_1,\ ...,\ \chi_n] \in \mathbb{R}^{n\times n}$ is a diagonal matrix containing the winding ratio of the winches.

The wrench matrix $\mathbf{W} \in \mathbb{R}^{m\times n}$ is a function of $\mathbf{x}$ and maps the EE velocities to the cable velocity vector. It is expressed as follows:

$$\mathbf{W} = \begin{bmatrix} \mathbf{d}_1 & ... & \mathbf{d}_n \\ {}^b\mathbf{R}_p\mathbf{a}_1 \times \mathbf{d}_1 & ... & {}^b\mathbf{R}_p\mathbf{a}_n \times \mathbf{d}_n \end{bmatrix}, \quad \mathbf{d}_i = \frac{\mathbf{b}_i - \mathbf{p} - {}^b\mathbf{R}_p\mathbf{a}_i}{\|\mathbf{b}_i - \mathbf{p} - {}^b\mathbf{R}_p\mathbf{a}_i\|_2}. \tag{3}$$

where $\mathbf{d}_i \in \mathbb{R}^u$ is unit vector of ith cable pointing from A_i to B_i. ${}^b\mathbf{R}_p$ is the rotation matrix of the mobile frame $\mathcal{F}_p$ with respect to the fixed frame $\mathcal{F}_b$.

The equations of motions in this paper are derived from Newton-Euler equations while considering the center of mass of the EE coincident with its geometric center, namely,

$$\mathbf{M}(\mathbf{x})\ \dot{\mathbf{t}} + \mathbf{C}(\mathbf{x}, \mathbf{t})\ \mathbf{t} = \mathbf{W}\boldsymbol{\tau} + \mathbf{w}_g + \mathbf{w}_e. \tag{4}$$

$\mathbf{M} \in \mathbb{R}^{m\times m}$ is the mass matrix of the moving platform. $\mathbf{C} \in \mathbb{R}^{m\times m}$ is the matrix of Coriolis and centrifugal forces. $\mathbf{t} \in \mathbb{R}^m$ is the twist vector of the EE. $\boldsymbol{\tau} \in \mathbb{R}^n$ is the cable tension vector. $\mathbf{w}_g \in \mathbb{R}^m$ is the wrench due to gravity acceleration. $\mathbf{w}_e \in \mathbb{R}^m$ amounts to the other wrenches applied to the mobile platform, except $\mathbf{w}_g$.

2.1. Determination of cable tensions

The determination of $\boldsymbol{\tau}$ is a function of the EE pose and the wrench that the latter should support. It is about solving the dynamic equilibrium equations for a given pose $\mathbf{x}$ of the EE, which can be described as follows:

$$\mathbf{W}\boldsymbol{\tau} + \mathbf{w}_{ex} = \mathbf{0}, \quad \mathbf{w}_{ex} = \mathbf{w}_g + \mathbf{w}_e - \mathbf{M}\ \dot{\mathbf{t}} - \mathbf{C}\ \mathbf{t}, \tag{5}$$

where $\mathbf{w}_{ex} \in \mathbb{R}^m$ denotes the external wrench. The cables can only pull and not push the EE. If the number of cables n is equal to the DOF m, the inversion of Eq. (5) is possible, as long as the wrench matrix $\mathbf{W}$ is not singular.

However, this tension set can present negative values. That means that one or more cable(s) may have to push the EE, which is not possible.

When $m<n$, Eq. (5) may have an infinite number of solutions. Therefore, the redundancy allows to select a solution amongst the infinite set cable tension vectors satisfying some criteria. The problem of force distribution presents one important design issue for redundant actuated CDPRs, which is the determination of feasible cable force distribution[1] [28, 29, 30, 31].

In what remains, the pre-compensation of the end-effector deflection will be based on the estimated cable elongations due to the applied tension set. Depending on the cable stiffness, different reference models for control will be defined: (*i*) rigid model, (*ii*) elasto-static model [25, 32] and (*iii*) elasto-dynamic model [26].

3. Feed-forward model-based control

The feed-forward model-based control uses a priori knowledge of the CDPR dynamics to improve the EE trajectory tracking by generating a pre-compensated control input. The pre-compensation unit is seen as an off-line compensation of the actuated joint displacement in such a way that after execution the EE follows the desired motion more accurately.

The feed-forward model-based control scheme is shown in Fig. 2. It is composed of a feed-forward block in which the inverse kinematic model is determined based on a CDPR reference model (Red block in Fig. 2). This latter is a predictive model of the dynamic behavior of the mechanism. Its input is the torque set-point $\boldsymbol{\zeta}_{rg} = \boldsymbol{\chi}\boldsymbol{\tau}_{rg} \in \mathbb{R}^n$, which is induced by the cable tensions $\boldsymbol{\tau}_{rg} \in \mathbb{R}^n$. It depends on the EE desired motion ($\mathbf{x}_{rg}$, $\mathbf{t}_{rg}$ and $\dot{\mathbf{t}}_{rg}$). It is determined based on the used tension distribution algorithm.

The output of the CDPR reference model is $\mathbf{q}_{ref} \in \mathbb{R}^n$, which represents the reference angular displacement of the motors. It depends on the chosen reference model. The joint angle vector $\mathbf{q}_{rg}$ is calculated based on $\mathbf{x}_{rg}$ with respect to Eq. (2). The joint velocity vector $\dot{\mathbf{q}}_{rg}$ and joint acceleration vector $\ddot{\mathbf{q}}_{rg}$ are the time derivatives of $\mathbf{q}_{rg}$. The vector $\mathbf{q}$ represents the measured joint angle vector of motors.

In this paper, it is assumed that all components of an actuator (motor, reducer and winch) are coaxial and all actuators are identical. Therefore, the motor torques vector $\boldsymbol{\zeta}_m \in \mathbb{R}^n$ is expressed as follows:

$$\boldsymbol{\zeta}_m = \boldsymbol{\zeta}_{corr} + \boldsymbol{\zeta}_f(\dot{\mathbf{q}}_{rg}) + \boldsymbol{\zeta}_{rg}, \tag{6}$$

The vector $\boldsymbol{\zeta}_{corr} = \mathbf{I}\mathbf{h}(t)$ corresponds to the torque of correction. The ith diagonal term of $\mathbf{I} = I\ \mathbb{1}^{n\times n}$ is the total actuator inertia matrix seen at their

[1] A cable force distribution will be said to be feasible in a particular configuration and for a specified set of wrenches if the cable tensions can counteract any external wrench of the specified set applied to the EE [27].

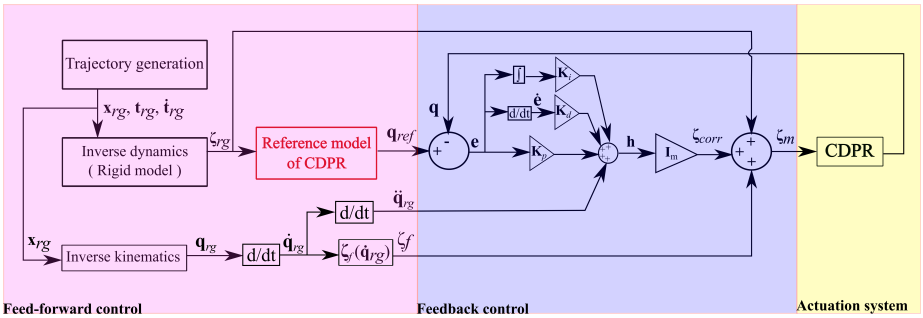

Figure 2: Feed-forward model-based PID control

exit.

$$I = r^2(I_{motor} + I_{reducer}). \tag{7}$$

I_{motor} is the inertia of the motor with brakes. $I_{reducer}$ is the inertia of the reducer. r is the gear-head (reducer) ratio. $\mathbf{h}(t)$ is defined by:

$$\mathbf{h}(t) = \ddot{\mathbf{q}}_{rg} + \mathbf{K}_p\ \mathbf{e} + \mathbf{K}_d\ \dot{\mathbf{e}} + \mathbf{K}_i \int_{t_i}^{t_i^+} \mathbf{e}\ dt, \tag{8}$$

where $\mathbf{e} = \mathbf{q}_{ref} - \mathbf{q}$ and $\dot{\mathbf{e}}$ are the angular displacement error vector and its time derivative, respectively. $\mathbf{K}_p \in \mathbb{R}^{n\times n}$ is the proportional gain matrix. $\mathbf{K}_d \in \mathbb{R}^{n\times n}$ is the derivative gain matrix. $\mathbf{K}_i \in \mathbb{R}^{n\times n}$ is the integrator gain matrix. $\boldsymbol{\zeta}_f \in \mathbb{R}^n$ is the friction torque vector, which is calculated with respect to the static friction model [33] as a function of the desired motion of the EE:

$$\boldsymbol{\zeta}_f(\dot{\mathbf{q}}_{rg}) = \boldsymbol{\zeta}_d\ \tanh(\dot{\mathbf{q}}_{rg}) + \boldsymbol{\zeta}_v\ \dot{\mathbf{q}}_{rg}. \tag{9}$$

$\boldsymbol{\zeta}_d \in \mathbb{R}^{n\times n}$ and $\boldsymbol{\zeta}_v \in \mathbb{R}^{n\times n}$ are two diagonal matrices containing the dry friction coefficients and the viscous friction coefficients of the actuators, respectively.

By calculating off-line an appropriate trajectory pre-compensation, the effects of the oscillatory dynamics are compensated. However, this may lead to a non robust control with respect to model uncertainties and a delay between the reference and the real CDPR behavior may occur. To handle this issue, the off-line feed-forward part should respect the findings in [34], dealing with a sensitivity analysis allowing to highlight the crucial parameters to be upstream identified. Accordingly, the control scheme of the CDPR is based on a robust model to uncertainties. This leads to the attenuation of errors coming from modeling and parameters uncertainties as shown for several industrial robots [35, 36].

3.1. Discrete-time control of CDPR

The correspondence between a CDPR and its control unit is described in Fig. 3. This organization of the equivalent control scheme is based on the findings in [15], dealing with a simulation tool of a discrete-time controlled CDPR. It

is composed of three units: (i) Actuation systems, (ii) Feedback controller and (iii) Feed-forward controller. Each unit of the equivalent control scheme is characterized by its own discretization time. Let Δt_a be the sampling time of the actuation system, which is a function of the feed-back controller frequency. Δt_b is the sampling time of the feed-forward unit. Δt_b is a function of the actuation system response. It is chosen smaller or equal to Δt_a. The feed-forward unit should be fast enough to avoid delays and divergence.

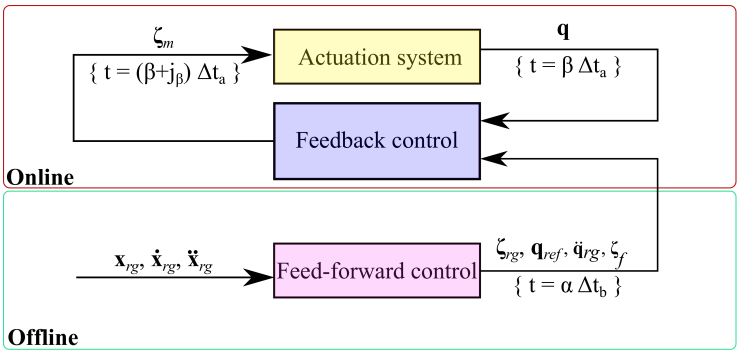

Figure 3: Equivalent control scheme: Discrete-time control

3.1.1. Actuation system

This model presents the actuators of the CDPR. Its input is the motor torque vector $\boldsymbol{\zeta}_m$ and its output is the measured angular coordinates $\mathbf{q}$ and velocities $\dot{\mathbf{q}}$ of the actuators. This measurement is obtained at each time $t = \beta \Delta t_a$.

3.1.2. Feedback control loop

This control loop permits the application of the control law mentioned in Eq. (6). The feedback control loop has a sampling time Δt_a. At each time $t = \beta \Delta t_a$, $\beta \in \mathbb{N}^+$,the loop calculates a new value for $\boldsymbol{\zeta}_m$, which is sent to the actuation model at time $t = (\beta + j_\beta)\Delta t_a$, at which a new measurement of $\mathbf{q}$ and $\dot{\mathbf{q}}$ is made. j_β is the delay between the generation of the control set-point by the feed-back controller and the reception of the encoder information. The value of $\boldsymbol{\zeta}_m$ is kept constant in the time interval $[(\beta + j_\beta)\Delta t_a \quad (\beta + j_\beta + 1)\Delta t_a]$.

3.1.3. Feed-forward control loop

This control loop aims to generate the modified trajectory. The input of this loop is the desired motion of the EE, which manifests in the desired pose $\mathbf{x}_{rg}$, twist $\mathbf{t}_{rg}$ and acceleration $\dot{\mathbf{t}}_{rg}$ of the moving platform. The output is the reference angular displacement $\mathbf{q}_{ref}$, the torque set-point $\boldsymbol{\zeta}_{rg}$, the friction torque $\boldsymbol{\zeta}_f$ and the angular acceleration $\ddot{\mathbf{q}}_{rg}$ generated from the desired motion of the moving-platform. The sampling time of the feed-forward control loop is Δt_b.

At each time $\alpha \Delta t_b$, a torque set-point $\boldsymbol{\zeta}_{rg}$ is calculated, coming from a cable tension distribution algorithm, with respect to the desired motion of the EE. The

pre-compensation of the trajectory is obtained by generating the joint angular displacement $\mathbf{q}_{ref}$ with respect to the chosen reference model of the CDPR.

$\mathbf{q}_{ref}$, $\boldsymbol{\zeta}_{rg}$, $\boldsymbol{\zeta}_f$ and $\ddot{\mathbf{q}}_{rg}$ are sent to the feedback control loop at each time $\alpha\Delta t_b$, $\alpha \in \mathbb{N}^+$. These vectors are kept constant in the time interval $[\alpha\Delta t_b \quad (\alpha+1)\Delta t_b]$.

3.2. Pre-compensation

The off-line pre-compensation strategy is applied to eliminate the trajectory tracking errors due to the robot compliance. This strategy is based on the anticipation of the joint errors and correcting them by modifying the reference actuated joint position $\mathbf{q}_{ref}$ as follows:

$$\mathbf{q}^j_{ref} = \mathbf{q}_{rg} - \delta\mathbf{q}^j_{mod}, \quad \delta\mathbf{q}^j_{mod} = \mathbf{q}^j_{mod} - \mathbf{q}_{rg}, \tag{10}$$

where j refers to the reference model control. It can be either "rg", "es" or "ed" to mention the *rigid*, *elasto-static* and *elasto-dynamic* models, resp. $\delta\mathbf{q}^j_{mod} \in \mathbb{R}^n$ is a vector of angular displacements errors, leading to trajectory tracking errors. This vector is calculated by simulating a CDPR model depending on the considered error sources. It anticipates the correction of the actuated joint angles $\mathbf{q}^j_{mod}$ with respect to the displacement vector $\mathbf{q}_{rg}$, which is calculated through the rigid model of CDPR and corresponds to the unstrained cable length $\mathbf{l}_{rg}$. The subtraction of $\delta\mathbf{q}^j_{mod}$ from $\mathbf{q}_{rg}$ generates a new reference input signal $\mathbf{q}^j_{ref}$ allowing the EE to track more accurately the desired trajectory.

It is noteworthy that $\delta\mathbf{q}^j_{mod}$ depends on the CDPR reference model used to calculate the vector $\mathbf{q}^j_{ref}$. To the best of our knowledge, two CDPR models have been used in the literature for the feed-forward model-based control of CDPRs with non-sagging cables: (*i*) rigid model and (*ii*) elasto-static model [25, 32]. As a consequence, one contribution of this paper deals with the use of the (*iii*) elasto-dynamic model of CDPRs for feed-forward control [26].

3.2.1. Rigid pre-compensation

The CDPR rigid model considers cables as rigid links. Here, the reference signal $\mathbf{q}^{rg}_{ref}$ anticipates neither the cable elongation nor the oscillatory motions of the EE. It is expressed as:

$$\mathbf{q}^{rg}_{ref} = \mathbf{q}_{rg}. \tag{11}$$

The PID feedback controller uses the motor encoders response $\mathbf{q}$, which is related to $\mathbf{l}_{rg}$. It should be noted that the cable elongations and EE oscillatory motions are not considered here, and as a consequence, cannot be rejected.

3.2.2. Elasto-static pre-compensation

The CDPR elasto-static model integrates a feed-forward cable elongation compensation [25]. At each sampling time $\alpha\Delta t_b$, each cable of the CDPR is isolated and its elongation is determined with respect to the discretized EE motion ($\mathbf{x}_{rg}$, $\mathbf{t}_{rg}$ and $\dot{\mathbf{t}}_{rg}$). Knowing the force applied on each cable, we estimate its elongation based on a cable tension model, which can be either linear or

non-linear [37]. In this paper, we consider the linear cable tension model, where the cable tension is linearly proportional to cable stiffness.

When $\mathbf{q}_{ref}^{rg}$ is used as a reference signal in the feedback control scheme, the EE displacement $\delta\mathbf{x}_{es}$ is obtained from cable elongation vector $\delta\mathbf{l}_{es}$. To compensate for the cable elongation effects, $\delta\mathbf{l}_{es}$ is converted into winch displacement $\delta\mathbf{q}_{mod}^{es}$, which estimates the joint error with respect to the rigid angular position $\mathbf{q}_{rg}$. Thus, the elasto-static reference angular displacement $\mathbf{q}_{ref}^{es}$ becomes:

$$\mathbf{q}_{ref}^{es} = \mathbf{q}_{rg} - \delta\mathbf{q}_{mod}^{es}. \tag{12}$$

The reference signal $\mathbf{q}_{ref}^{es}$ corresponds to a fake position of the EE for the cable elongation compensation. Here, under the effect of cable elongations, the reference EE pose is estimated to achieve the desired pose. Although the elasto-static reference model takes into account the cable elongations, the non-compensation for the EE pose errors due to the cable interaction with the whole system and elasto-dynamic behavior is not considered.

3.2.3. Elasto-dynamic pre-compensation

The CDPR elasto-dynamic model takes into account the oscillatory and dynamic behavior of the EE due to cable elongations. Here, the cables are no-longer isolated and are affected by the EE dynamic behavior. The real EE pose is expressed as: $\mathbf{x}_{ed} = \mathbf{x}_{rg} + \delta\mathbf{x}_{ed}$. The EE displacement $\delta\mathbf{x}_{ed}$ leads to variations in both cable lengths and cable tensions. Indeed, the ith cable tension $\boldsymbol{\tau}_{ed}^{i}$ obtained from the elasto-dynamic model differs from $\boldsymbol{\tau}_{rg}^{i}$ calculated based on a tension distribution algorithm:

$$\tau_{ed}^{i} = \tau_{rg}^{i} + \delta\tau_{ed}^{i} = ES\ \frac{\delta l_{ed}^{i}}{\delta l_{ed}^{i} + l_{rg}^{i}}, \tag{13}$$

where E is cable modulus of elasticity and S is its cross sectional area. δl_{ed}^{i} is the ith cable elongation assessed by considering cable elasticity and oscillations. The EE pose $\mathbf{x}_{ed}$ is calculated through the direct elasto-dynamic model thanks to MATLAB® routine ode45 by coupling Eq. (4) and Eq. (13). The cable elongation vector $\delta\mathbf{l}_{ed}$ is converted into $\delta\mathbf{q}_{mod}^{ed}$, which corrects the angular position vector $\mathbf{q}_{rg}$. Therefore, the elasto-dynamic reference angular displacement $\mathbf{q}_{ref}^{ed}$ becomes:

$$\mathbf{q}_{ref}^{ed} = \mathbf{q}_{rg} - \delta\mathbf{q}_{mod}^{ed}. \tag{14}$$

The proposed control strategy based on the elasto-dynamic model leads to a feed-forward controller for EE oscillatory motion compensation in addition to the conventional rigid body feedback while considering the motor encoder measurements.

3.3. Controller tuning

No matter the reference model used in the control scheme (see Fig. 2), the controller tuning methodology is the same. Applying the Laplace transform to

the tracking error differential Eq. (8), and assuming zero initial conditions, we obtain for each drive:

$$e(s)(s^3 + K_p\ s + K_d\ s^2 + K_i) = 0. \tag{15}$$

Equation. (15) can be rewritten as follows:

$$e(s)(s + \Upsilon_n)(s^2 + 2\upsilon\Upsilon_n\ s + {\Upsilon_n}^2) = 0, \tag{16}$$

with $K_p = (2\upsilon+1)\Upsilon_n^2$, $K_d = (2\upsilon+1)\Upsilon_n$ and $K_i = \upsilon_n^3$. This differential equation expresses the dynamic behavior of the closed-loop tracking error in response to a perturbation. This corresponds to a first-order system followed by a second-order system. Since the parameters υ and Υ_n are strictly positive, the system is always stable.

To obtain the fastest answer without oscillation, $\upsilon = 1$ is chosen. Thus, a third order system with a triple real pole is obtained. In this case, the PID gains become:

$$K_p = 3\Upsilon_n^2,\ K_d = 3\Upsilon_n,\ K_i = \Upsilon_n^3. \tag{17}$$

Note that K_p, K_d and K_i are all functions of Υ_n. A simple and effective method is to select Υ_n is twice the breaking pulse $\Upsilon_c = \dfrac{k_t\ k_e}{\varpi\ I}$ of the motors where ϖ is the resistance of the motor armature, k_e is the counter-electromotive force coefficient and k_t represents the electromagnetic torque coefficient of the motor.

4. Control of a 3-DOF spatial CDPR with a point-mass end-effector

This section aims to describe the CDPR prototype to be used to check the relevance of the elasto-dynamic feed-forward control with respect to the classical rigid and elasto-static ones. The variations in the EE position error along a trajectory are numerically and experimentally studied on the CREATOR prototype located at LS2N. The CDPR configuration used for the tests is composed of three cables and a point-mass EE. The EE is requested to track the linear path defined in Section 4.2.

4.1. Test bench

Figure 5 describes the equivalent architecture of the CREATOR prototype. The test bench is prepared under the assumption that cables are elastic and keep linear shape along a trajectory. The EE and pulleys are considered as points. To provide this configuration, some precautions are taken into account on the experimental test bench to provide the particular configuration of the CREATOR prototype:

- The CREATOR prototype is actuated by three Parker™ motors[2] with gear-heads[3] connected to 3D printed winches. The motors characteristics

[2] Parker™ SMB/SME Brushless servo motor series. Ref: SMEA 60601- 489IZ64S54.
[3] Parker™ Economical Planetary Gearheads - PE. Ref: PE3-008-10M040/063/09/20.

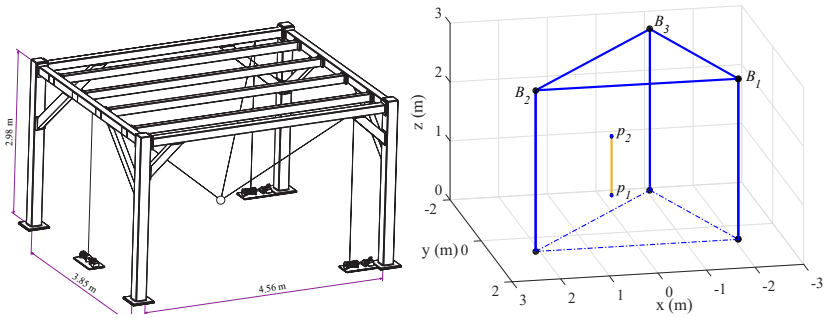

(a) (b)

Figure 4: (a) CREATOR prototype CAD diagram (b) End-effector desired path in $\mathcal{F}_b$

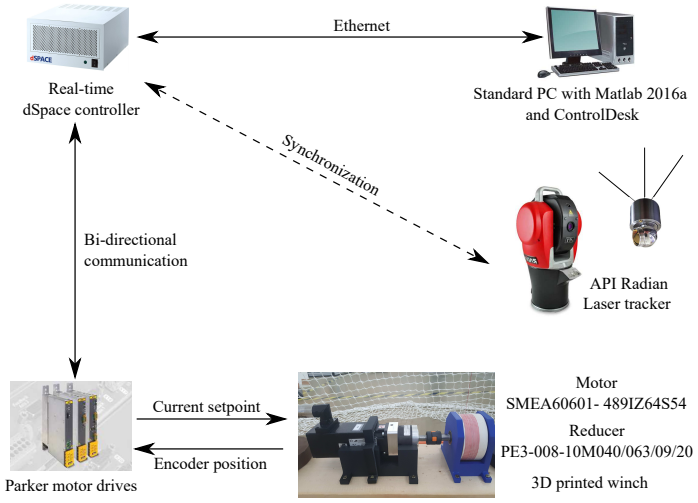

Figure 5: Equivalent architecture of the CREATOR protype

are given in Tab. 1. Each motor is connected to a Parker™ motor drive, which communicates with the dSpace™ controller through bi-directional real-time links.

Table 1: Characteristics of the CREATOR actuators and the gains of the PID controller

Parameter (Unit)	I_{motor} (kg.m^2)	$I_{reducer}$ (kg.m^2)	I (kg.m^2)	k_e (Vrms.s/rad)	ϖ (Ohm)	r
Value	42.5e-6	6.5e-6	0.0031	0.48	12.8	8

The friction torques of the actuators are identified with respect to the static friction model [33] by incrementing the joint angular velocity. The first move of the actuator corresponds to the dry friction torque ζ_d. As we

Table 2: K_p, K_d and K_i gains of the PID controller

Gain	K_p	K_d	K_i
Value	1125.8	58.12	7269.60

do not have an accurate measurement of the motor torques, we suppose that the viscous friction torque is zero. Here, the dry friction value is ζ_d=0.14 N.m.

- The winch is 3D printed and it is mounted to the reducer axis. Its pitch is equal to 2 mm and its radius is equal to 50 mm.

- 3D printed pieces are used as pulleys of the CREATOR protype (See Fig. 6). They were designed in such a way that their exit amount to a point. The entrance of the pulley is conical and their exit is a hole of 3 mm of diameter. Grease is added inside the pulley to reduce friction between the cable and the pulley.

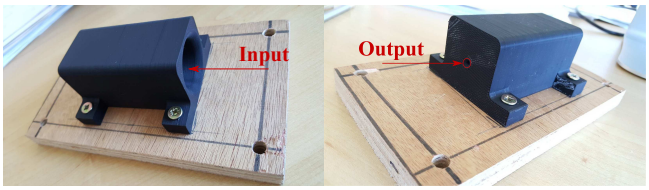

(a) (b)

Figure 6: 3D-printed pulleys used for the CREATOR protype

- The robustness analysis in [34] highlighted the high effect of the cables elasticity onto the dynamic and oscillatory motions of the EE. The CREATOR cables are made up of eight threads of polyethylene fiber with a diameter of 0.5 mm. These cables were experimentally upstream identified. The identification method is described in [37]. The absolute uncertainties in the applied force and resulting elongation measurements from the test bench outputs are estimated to be $\pm$ 1 N and $\pm$ 0.03 mm, respectively [37]. The resulting modulus of elasticity of the cable is equal to 70 $\pm$ 1.51 GPa.

  The following trajectory tracking experiments will confirm a good identification of the modulus of elasticity. This is shown through the measurement of a natural frequency $\approx$ 3.5 Hz, which corresponds to the calculated natural frequency (3.67 Hz) while using the identified modulus of elasticity. The reference [38] was used for the calculation of the natural frequencies of the CDPR. It is based on the global stiffness matrix of the CDPR. The natural frequencies of the system are obtained by solving the eigenvalue problem of the linearized free vibration equation driven by the generalized stiffness matrix of the CDPR and the mass matrix of the end-effector.

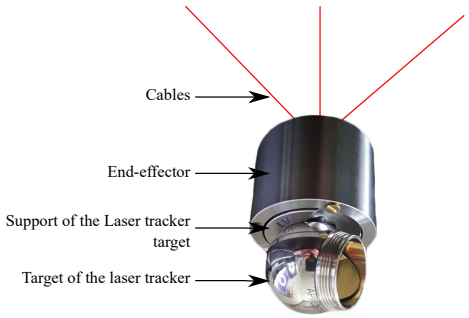

Figure 7: End-effector and laser tracker target

- The EE was designed such that it is close to a point-mass. It is a steel machined cylinder with a hole that crosses vertically and a conical hole on its top surface. This makes the cables to intersect at the same point.

  The magnetic support of the laser tracker target is connected to the EE at its bottom part. The laser tracker target is then connected to this magnetic support, Fig. 7. The acquired information from the laser tracker presents measurements with respect to the target center. An offset with respect to the EE gravity center is considered to get the appropriate trajectory tracking measurements.

  The total mass of the EE used for the control gathers its own mass plus the mass of the laser tracker target and its magnetic support. The total mass of the EE is equal to 0.780 kg.

- The command of the CREATOR prototype is implemented in a host PC through a software interface generated by ControlDesk®[4]. This latter enables the real-time implementation of the control schemes, created with Matlab-Simulink®, in the dSpace™ control unit. The control sampling times Δt_a and Δt_b are considered equal: $\Delta t_a = \Delta t_b = 1$ ms.

- An API Radian laser tracker was used to define the base frame $\mathcal{F}_b$. A circle plane passing through points B_1, B_2 and B_3 is created and is projected on the floor to create the base frame, whose origin is the circle center. All the measurements are expressed in that frame. Moreover, the laser tracker is used to measure the pose of the EE along the tracked trajectory in the global base frame $\mathcal{F}_b$. The static measurement accuracy of the used laser tracker is ± 10 μm. The measurement start signal is synchronized with the control signal through the dSpace controller.

[4]ControlDesk is the dSPACE experiment software for seamless electronic control unit development. It performs all the necessary tasks in a single working environment, from the start of experimentation right to the end.

4.2. Trajectory generation

Before running trajectory tracking, a pre-compensation of the EE static deflection is performed while adopting the CDPR control based on its elasto-static and the elasto-dynamic models, respectively. Thus, the static deflection due to the EE weight is compensated by correcting the joint angular displacement leading to trajectory tracking error.

A linear path along the vertical axis with a 5-th degree polynomial motion profile is considered. It goes from the initial position $\mathbf{p}_1$ to the final position $\mathbf{p}_2$, 1 m high along z-axis, during t_f=3 s. A pause equal to t_f at the final pose is considered. The effects of the EE residual oscillations are easily detected during the steady-state phase. Therefore, the EE trajectory is parametrized as follows:

$$\mathbf{p}(t) = \mathbf{p}_1 + \alpha(t)\ (\mathbf{p}_2 - \mathbf{p}_1); \quad t \in [0 \quad t_f], \tag{18a}$$

$$\mathbf{p}(t) = \mathbf{p}_2; \quad t > t_f. \tag{18b}$$

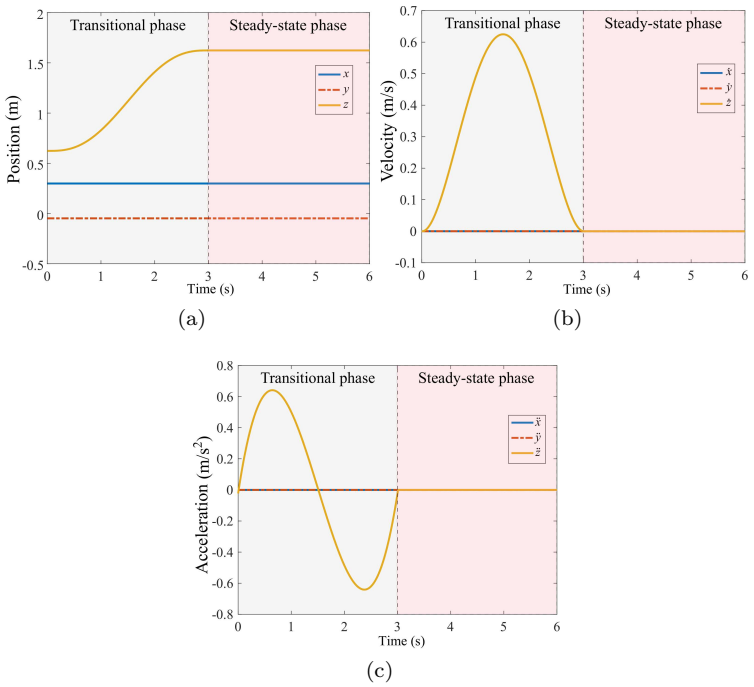

Figure 8: Desired (a) Position (b) Velocity and (c) Acceleration profiles of the end-effector

The fifth degree polynomial for the linear path is expressed as:

$$\alpha(t) = \beta_5\ t^5\ + \beta_4\ t^4\ +\ \beta_3\ t^3\ +\ \beta_2\ t^2\ +\ \beta_1\ t + \beta_0, \tag{19}$$

where $\beta_5 = \dfrac{6}{t_f^5}$, $\beta_4 = \dfrac{-15}{t_f^4}$, $\beta_3 = \dfrac{10}{t_f^3}$, $\beta_2 = 0$, $\beta_1 = 0$ and $\beta_0 = 0$. These values are chosen such that the velocity and acceleration of the EE are null at the beginning and the end of the trajectory as shown in Figs. 8b and 8c.

5. Numerical simulations

The three control schemes under study were simulated through Matlab-Simulink® to analyze their relevance. To assess the performances of different control laws, the CDPR elasto-dynamic model is used to estimate the EE real position as it is the closest one to the real CDPR with non sagging cables. This is to be confirmed in Section 6. Therefore, it is used to predict the real behavior of the CDPR. The input of this model is $\boldsymbol{\zeta}_m$, which leads to the Cartesian coordinate vector $\mathbf{p}_{ed}^m$ of the EE position. The trajectory error is defined as: $\delta\mathbf{p}(t) = \mathbf{p}_{ed}^m(t) - \mathbf{p}_{rg}(t)$.

Figure 9b shows the norm $\|\delta\mathbf{p}\|$ of the end-effector trajectory tracking error when the proposed model-based feed-forward control law is applied. The three CDPR models are successively used to generate the reference signal. Figure 9a illustrates the end-effector trajectory tracking error δz along the z-axis, which is the main one as the CDPR under study is assembled in a suspended configuration and its end-effector tracks a vertical trajectory. The red (green, blue, resp.) curve depicts the end-effector trajectory tracking error when the elasto-dynamic (elasto-static, rigid, resp.) model is used as a reference model.

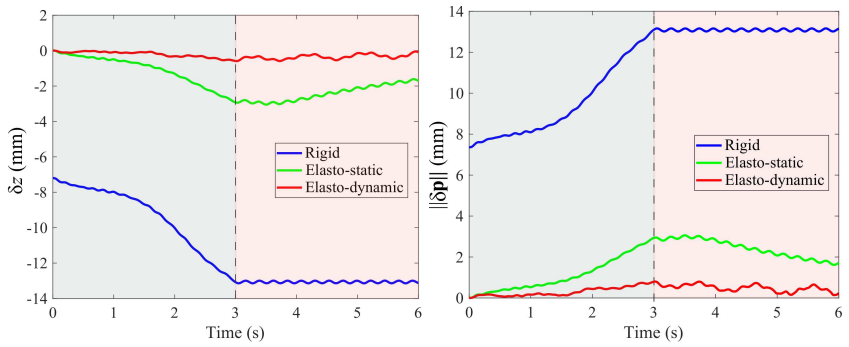

(a) (b)

Figure 9: (a) Position error of the end-effector along the z-axis (b) 2-norm of the end-effector Cartesian trajectory tracking error vector

The position error norm $\|\delta\mathbf{p}\|$ while using the rigid model as a reference for the feed-forward at time $t = 3$ s is equal to 13.14 mm. This value is equal to 2.18 mm when the elasto-static model is used as a reference for the feed-forward,

which represents a relative difference of 83 % with respect to the rigid control[5]. The position error norm $\|\delta\mathbf{p}\|$ while using the elasto-dynamic model as a reference for the feed-forward at time $t = 3$ s is equal to 0.58 mm, which represents a relative difference of 95 % with respect to the rigid control.

This shows a good improvement of the moving-platform positioning accuracy at the end of the trajectory through the elasto-dynamic compensation comparing to classical feed-forwards. The trajectory tracking error is also reduced significantly with the CDPR elasto-dynamic control[6] compared to the classical feed-forward model-based control schemes. This is due to the fact that the elasto-dynamic control compensates not only the static errors due to cable elongations but also the oscillatory behavior of the moving-platform. Next, experimental results are performed to verify numerical ones.

6. Experimental results

6.1. Experimental setup

The experimental procedure used to verify the relevance of the elasto-dynamic model-based control is the following:

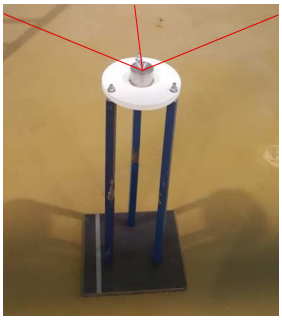

Figure 10: Experimental setup: Non-suspended initial pose of the end-effector

- A support for the EE, shown in Fig. 10, is placed on its desired initial position. The base plate of this support is 3D printed and is connected to a steel block through steel square tubes. This base is a negative form of the EE. The support is useful to define the relationship between actuated angles and the corresponding unstrained cable lengths. Besides, it provides the same initial pose for the EE for the different experiments.

  As shown in Fig. 10, the EE is first located on the support. Thus, it is in the non-suspended initial pose and it undergoes neither the external effects nor its stiffness. The absolute position of the EE is measured in that non-suspended configuration.

[5]"rigid control" refers to "rigid model-based control of CDPR"
[6]"elasto-dynamic control" refers to "elasto-dynamic model-based control of CDPR"

- Modify cable lengths such that their tension is a minimum while keeping cables without sag. Then, lock the motors.
- The support is removed and the EE becomes suspended under the effect of its own weight subjected to cable elasticity. Then, the suspended position of the EE is measured.
- A command is generated through ControlDesk® in combination with Matlab-Simulink®. It makes the EE move along a straight line.
- When the elasto-static or elasto-dynamic models are used as references for the control, a compensation of the static deflection is performed before starting the trajectory. This is done through smooth angular displacements of joints corresponding to the correction of the static deflection.

6.2. Static analysis

The ideal initial position of the EE corresponds to the initial rigid position $\mathbf{p}_{rg}(t = 0^- \ s)$. This latter is measured when the EE is located on the support in the absence of the stiffness effect; $\mathbf{p}_{rg}(t = 0^- \ s) = [0.299, \ -0.047, \ 0.623]$ m.

Three tests are performed to check the positioning repeatability. This is done by suspending the EE and measuring its corresponding static deflection. The suspended position $\mathbf{p}_{es}(t = 0^- \ s)$ of the EE is measured when the support is removed and the EE is suspended under the effect of its own weight.

Table 3 displays the static deflection $\|\mathbf{dp}\|$ with respect to the same non-suspended rigid position $\mathbf{p}_{rg}(t = 0^- \ s)$ for different tests. The EE presents a different static deflection for each test. This depends on the initial tensions on the cables when the EE is in its ideal initial position. The absence of tension sensors makes it hard to start the experiments with zero cable tensions without sag, leading to different static deflections.

Table 3: Experimental data: Static deflection of the end-effector before compensation

Experience	Test 1	Test 2	Test 3
Static deflection $\|\mathbf{dp}\|$ (mm)	9.00	6.32	8.30

The position repeatability is not good enough, so for each test we obtain a different position for the EE. Indeed, the trajectory does not start with the same position for the different tests. Comparing the control laws by comparing the absolute trajectory errors will not project the true improvement of the accuracy as the different trajectories do not start with the same static error.

For this fact, we propose to define a new reference $\mathbf{p}^*$ to be used for the determination of the trajectory error. $\mathbf{p}^*$ is defined as described in Sec. 4.2 starting from the compensated position, where $\mathbf{p}^*(t = 0 \ s) = \mathbf{p}_{es}(t = 0^+ \ s)$. This allows to compensate the static error for the different tests at the start time of the trajectory. This static error should be seen at the end of the trajectory.

6.3. Trajectory tracking

The trajectory error $\delta\mathbf{p}$ is defined as the difference between the measured trajectory $\mathbf{p}$ and the reference one $\mathbf{p}^*$: $\delta\mathbf{p}(t) = \mathbf{p}(t) - \mathbf{p}^*(t)$. Figure 12d shows the norm of the EE trajectory tracking error $\|\delta\mathbf{p}\|$ when the proposed feed-forward control law is applied while using successively the three CDPR models to generate the reference signal. Figure 12c illustrates the EE trajectory tracking error along the z-axis δz, which is the main one as the CDPR under study is assembled in a suspended configuration and the trajectory is vertical. The red (gree, blue, resp.) curve depicts the EE trajectory tracking error when the elasto-dynamic (elasto-static, rigid, resp.) model is used as a reference.

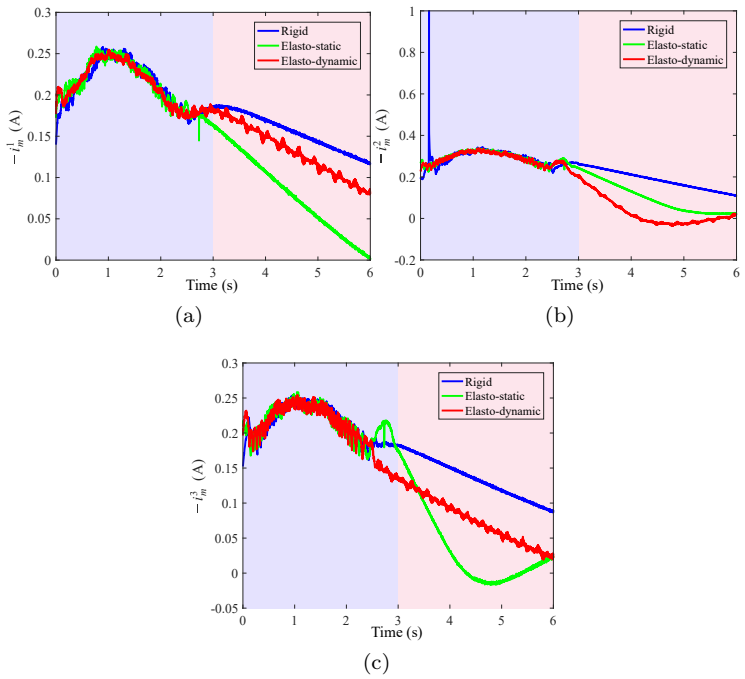

Figure 11: Experimental results: Current set-points (a) i_m^1, (b) i_m^2 and (c) i_m^3

Figure 11 shows the set-point of current $\mathbf{i}_m = [i_m^1, i_m^2, i_m^3]^T$ sent to the actuators, which is an image of torque set-point $\boldsymbol{\zeta}_m$. It is noteworthy that the elasto-dynamic current set-point takes into account the oscillatory behavior on the contrary to classical feed-forwards.

As one can see, the set-point of current is not constant during the steady-state phase. This reflects the integrator effect of the PID controller as its input is never zero. In addition, the torques $\boldsymbol{\zeta}_{rg}$ and $\boldsymbol{\zeta}_f$ do not compensate totally the gravity and friction effects as they are obtained by identification, which is influenced by uncertainties.

While applying $\mathbf{i}_m$, the resulting trajectory error of the EE is plotted in

Fig. 12. It is worth noting in these plots that the frequency of EE vibrations is equal to 3.5 Hz, which is close to the calculated first natural frequency f_1=3.67 Hz. A good identification of the modulus of elasticity, respecting the uncertainty analysis conclusions, is confirmed.

From Figs. 11 and 12, the delay j_β can be determined. When the rigid model of the CDPR is used, a current discontinuity at time 2.53 s is depicted. This leads to a discontinuity in $\|\delta\mathbf{p}\|$ at time 2.68 s, which corresponds to j_β^{rg}=0.15 s. When the elaso-static model of the CDPR is used, a current discontinuity at time 2.73 s is depicted. This leads to a discontinuity in $\|\delta\mathbf{p}\|$ at time 2.87 s, which corresponds to j_β^{es}=0.14 s. When the elasto-dynamic model of the CDPR is used, a current discontinuity at time 2.57 s is depicted. This leads to a discontinuity in $\|\delta\mathbf{p}\|$ at time 2.70 s, which corresponds to j_β^{ed}=0.13 s.

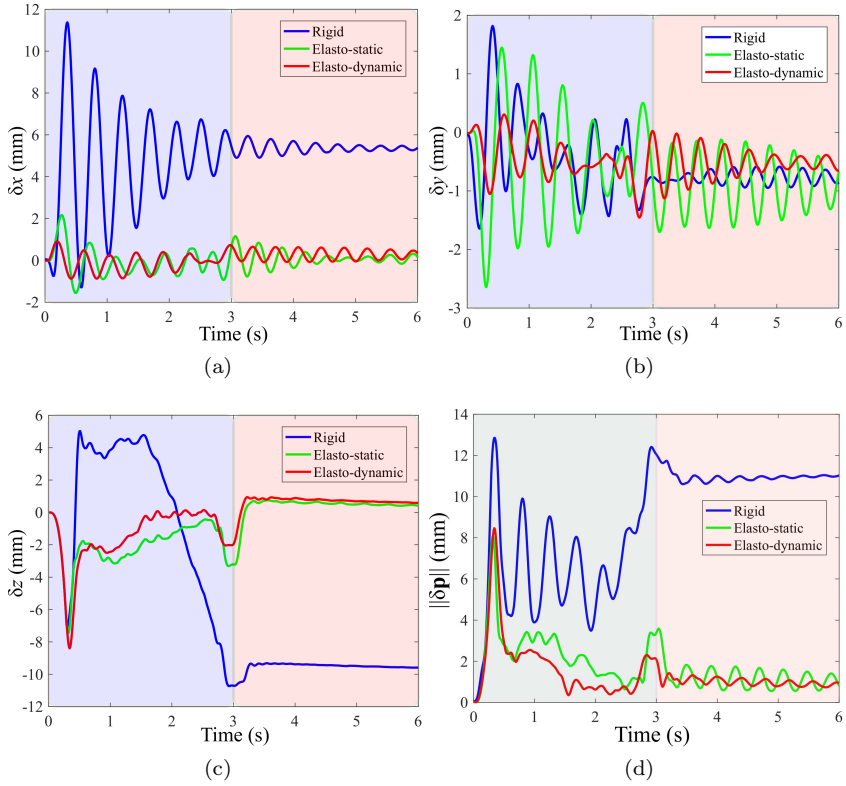

Figure 12: Experimental results: Position error along (a) x-axis, (b) y-axis and (c) z-axis of the end-effector (d) Position error norm

6.3.1. Transitional phase

At time t=0 s, the trajectory error is set to be zero. In fact, the static error is reported artificially to the end of the trajectory as the real trajectory of the EE is compared to the modified rigid one $\mathbf{p}^*$.

Note that the end-effector position errors along x-axis and z-axis are mainly due to the end-effector swaying, the end-effector being not a point-mass. Besides, the experimental validations were performed with a CDPR suspended configuration, which leads to a low horizontal stiffness of the end-effector. This may lead to end-effector swaying and large horizontal oscillations under the effect of external disturbances, especially when using a light end-effector.

As shown in Fig. 12, the trajectory tracking error norm $\|\delta\mathbf{p}\|$ while using the rigid model as a reference for the feed-forward at time t=3 s is equal to 12.05 mm. This value is equal to 3.45 mm when the elasto-static model is used as a reference for the feed-forward, which represents a relative difference of 71 % with respect to the rigid control. The position error norm $\|\delta\mathbf{p}\|$ while using the elasto-dynamic model as a reference for the feed-forward at time t=3 s is equal to 2.01 mm, which represents a relative improvement of 83 % with respect to the rigid control.

This confirms a better improvement of the EE positioning errors through the elasto-dynamic compensation comparing to classical feed-forwards. This is due to the correction of static errors through the compensation of cable elongations and the EE oscillatory effects.

6.3.2. Steady-state phase

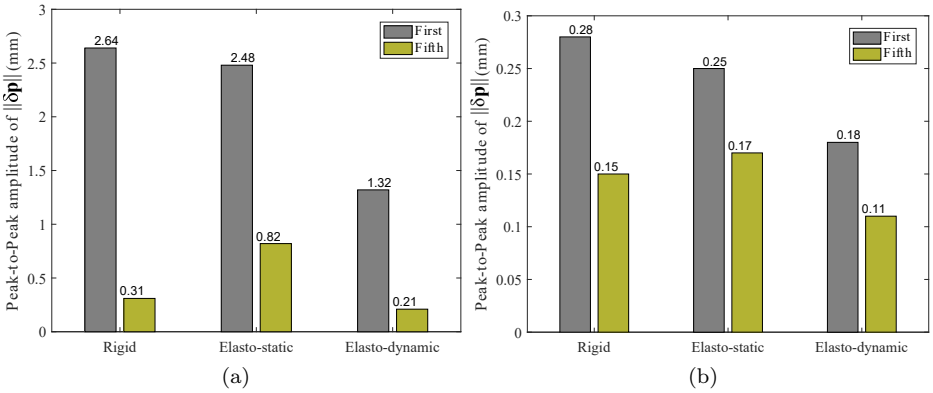

Figure 13: (a) Experimental, (b) Numerical First and fifth Peak-to-Peak amplitudes of $\|\delta\mathbf{p}\|$

As shown in Fig. 12, at time t=3 s, the EE achieves its final position and then oscillates. Fig. 13 depicts that when the rigid control is used, the first Peak-to-Peak amplitude of residual vibrations is equal to 2.64 mm. This value is equal to 2.48 mm when the elasto-static model is used as a reference for the feed-forward, which represents a relative difference of 6 % with respect to the rigid control. When the elasto-dynamic model is used as a reference for the feed-forward, the first Peak-to-Peak amplitude of residual vibrations is equal to 1.32 mm, which represents a relative improvement of 50 % with respect to the rigid control.

The fifth Peak-to-Peak amplitude of residual vibrations is equal to 0.31 mm when the rigid model is used as a reference for the feed-forward. This value is equal to 0.82 mm when the elasto-static model is used as a reference for the feed-forward. The fifth Peak-to-Peak amplitude of residual vibrations is equal to 0.21 mm when the elasto-dynamic control is used, which represents a relative improvement of 32 % with respect to the rigid control.

Note that the experimental first Peak-to-Peak amplitude of residual vibrations is ≈10 times higher than the numerical one as shown in Fig. 13. This is due to the oscillatory behavior of the EE, which is a non-perfect point-mass that may swing out along the trajectory.

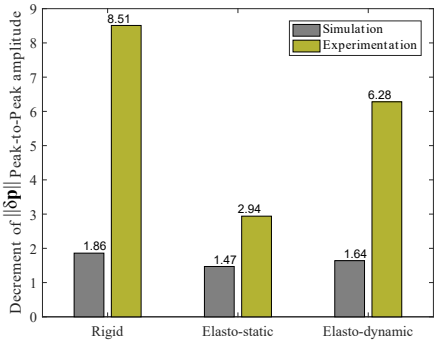

Figure 14: Decrement of the Peak-to-Peak amplitudes of $\|\delta\mathbf{p}\|$ during the steady-state phase

The decrement of residual vibrations is used to define the performance indexes of control laws with respect to residual vibration reduction. It is defined as the ratio between the first and the fifth Peak-to-Peak amplitudes. Figure 14 shows the decrement of the Peak-to-Peak amplitudes of $\|\delta\mathbf{p}\|$ during the steady-state phase. This decrement is equal to 6.28 (2.94, 8.51, resp.) when the elasto-dynamic (elasto-static, rigid, resp.) model is used as a reference for the feed-forward. The decrement of the Peak-to-Peak amplitudes of $\|\delta\mathbf{p}\|$ obtained through experiments presents the same tendency than the numerical one. However, this experimental decrement is higher than the simulated ones. This means that some damping effects were not taken into consideration in simulations. A part of the damping may occur in the pulley system as the different control laws take into account neither the pulley friction nor the cable sliding into the pulley grooves. Furthermore, the winch friction torques are not well identified as the drums are 3D printed, leading to uncertainties. However, there is a clear improvement of trajectory tracking and vibration attenuation.

7. Conclusion

This paper proposed a model-based feed-forward control strategy for CDPRs. The elasto-dynamic model of CDPRs was proposed to anticipate the full dynamic behavior of the mechanism including the vibratory effects, cable elongations and

their interaction with the whole system to compensate them. The integration of tension distribution makes the proposed control scheme valid for every configuration of CDPRs. The comparison between the trajectory tracking errors obtained when using the proposed elasto-dynamic model and the trajectory tracking errors obtained while using the classical rigid and elasto-static ones as control references shows meaningful differences. The different experimental

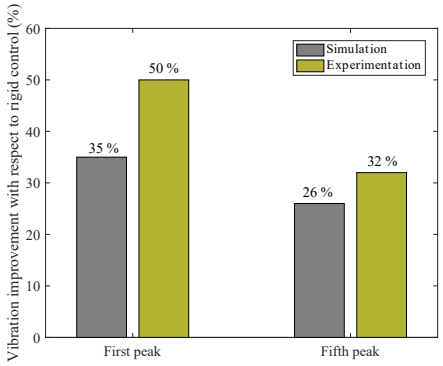

Figure 15: Vibration improvement of the elasto-dynamic control with respect to rigid control

results confirm the numerical ones stating that the elasto-dynamic control leads to better trajectory tracking and better attenuation of residual vibrations of the EE than the conventional elasto-static and rigid controls. Numerical results mention that elasto-dynamic control leads to an improvement of 35 % for the first Peak-to-Peak amplitude and an improvement of 26 % for the fifth one with respect to the rigid control. Accordingly, experimentations confirm this improvement as shown in Fig. 15. Indeed, the elasto-dynamic control leads to an improvement of 50 % for the first Peak-to-Peak amplitude and an improvement of 32 % for the fifth one with respect to the rigid control. As a conclusion, the elasto-dynamic control scheme introduced in this paper is a good way to attenuate CDPR residual vibrations. The proposed control strategy was experimentally for a CDPR prototype where cable elasticity arises. Future research work should focus on the cable dynamic sagging modeling, which may be more relevant for other CDPR configurations. Such a case will occur when cable sagging becomes more influential than cable elasticity.

8. Nomenclature

DOF : Degree-Of-Freedom.

CDPR : Cable-Driven Parallel Robot.

$\mathcal{F}_b = \{O,\ x_b,\ y_b,\ z_b\}$: Base frame.

$\mathcal{F}_p = \{P,\ x_p,\ y_p,\ z_p\}$: End-effector frame.

${}^{b}\mathbf{R}_{p}$: Rotation matrix of $\mathcal{F}_p$ with respect to $\mathcal{F}_b$.

n : Number of cables.

m : Total number of DOF.

$\mathbf{a}_i$: Cartesian coordinate vectors of anchor points A_i expressed in $\mathcal{F}_p$.

$\mathbf{b}_i$: Cartesian coordinate vectors of exit points B_i expressed in $\mathcal{F}_b$.

$\mathbf{x}$: End-effector pose vector expressed in $\mathcal{F}_b$.

$\mathbf{p}$: End-effector position vector.

$\mathbf{o}$: End-effector orientation vector.

$\boldsymbol{\zeta}_m$: Motor torque set-point vector.

$\boldsymbol{i}_m$: Current set-point vector.

$\boldsymbol{\tau}$: Cable tension vector.

$\mathbf{q}$: Angular displacement vector.

$\mathbf{l}$: Cable length vector.

$\boldsymbol{\chi}$: Diagonal matrix containing the winding ratio of the winches.

[1] T. Dallej, M. Gouttefarde, N. Andreff, R. Dahmouche, P. Martinet, Vision-based modeling and control of large-dimension cable-driven parallel robots, in: IEEE/RSJ International Conference on Intelligent Robots and Systems (IROS), 2012, IEEE, 2012, pp. 1581–1586.

[2] D. Q. Nguyen, M. Gouttefarde, F. Pierrot, et al., On the analysis of large-dimension reconfigurable suspended cable-driven parallel robots, in: IEEE International Conference on Robotics and Automation (ICRA), 2014, IEEE, 2014, pp. 5728–5735.

[3] J.-B. Izard, A. Dubor, P.-E. Hervé, E. Cabay, D. Culla, M. Rodriguez, M. Barrado, On the improvements of a cable-driven parallel robot for achieving additive manufacturing for construction, in: Cable-Driven Parallel Robots, Springer, 2018, pp. 353–363.

[4] J. Lamaury, M. Gouttefarde, A. Chemori, P.-E. Hervé, Dual-space adaptive control of redundantly actuated cable-driven parallel robots, in: IEEE/RSJ International Conference on Intelligent Robots and Systems (IROS), 2013, IEEE, 2013, pp. 4879–4886.

[5] S. K. Agrawal, V. N. Dubey, J. J. Gangloff, E. Brackbill, V. Sangwan, Optimization and design of a cable driven upper arm exoskeleton, in: ASME 2009 International Design Engineering Technical Conferences and Computers and Information in Engineering Conference, American Society of Mechanical Engineers, 2009, pp. 3–10.

[6] R. Yao, X. Tang, J. Wang, P. Huang, Dimensional optimization design of the four-cable-driven parallel manipulator in fast, IEEE/ASME Transactions On Mechatronics 15 (6) (2010) 932–941.

[7] L. Gagliardini, S. Caro, M. Gouttefarde, A. Girin, Discrete reconfiguration planning for cable-driven parallel robots, Mechanism and Machine Theory 100 (2016) 313–337.

[8] L. Gagliardini, S. Caro, M. Gouttefarde, A. Girin, A reconfiguration strategy for reconfigurable cable-driven parallel robots., in: ICRA, 2015, pp. 1613–1620.

[9] L. D. Viet, Y. Park, A cable-passive damper system for sway and skew motion control of a crane spreader, Shock and Vibration 2015.

[10] X. Weber, L. Cuvillon, J. Gangloff, Active vibration canceling of a cable-driven parallel robot using reaction wheels, in: IEEE/RSJ International Conference on Intelligent Robots and Systems, 2014, IEEE, 2014, pp. 1724–1729.

[11] H. Jamshidifar, B. Fidan, G. Gungor, A. Khajepour, Adaptive vibration control of a flexible cable driven parallel robot, IFAC-PapersOnLine 48 (3) (2015) 1302–1307.

[12] B. Zi, B. Duan, J. Du, H. Bao, Dynamic modeling and active control of a cable-suspended parallel robot, Mechatronics 18 (1) (2008) 1–12.

[13] A. Pott, H. Mütherich, W. Kraus, V. Schmidt, P. Miermeister, A. Verl, Ipanema: a family of cable-driven parallel robots for industrial applications, in: Cable-Driven Parallel Robots, Springer, 2013, pp. 119–134.

[14] J. I. A. Cuevas, É. Laroche, O. Piccin, Assumed-mode-based dynamic model for cable robots with non-straight cables, in: Cable-Driven Parallel Robots, Springer, 2018, pp. 15–25.

[15] J.-P. Merlet, Simulation of discrete-time controlled cable-driven parallel robots on a trajectory, IEEE Transactions on Robotics.

[16] E. Laroche, R. Chellal, L. Cuvillon, J. Gangloff, A preliminary study for h_∞ control of parallel cable-driven manipulators, in: Cable-Driven Parallel Robots, Springer, 2013, pp. 353–369.

[17] M. A. Khosravi, H. D. Taghirad, Dynamic modeling and control of parallel robots with elastic cables: singular perturbation approach, IEEE Transactions on Robotics 30 (3) (2014) 694–704.

[18] M. Khosravi, H. D. Taghirad, Stability analysis and robust pid control of cable driven robots considering elasticity in cables, AUT Journal of Electrical Engineering 48 (2) (2016) 113–126.

[19] M. A. Khosravi, H. D. Taghirad, Dynamic analysis and control of cable driven robots with elastic cables, Transactions of the Canadian Society for Mechanical Engineering 35 (4) (2011) 543–558.

[20] M. A. Khosravi, H. D. Taghirad, Dynamic analysis and control of fully-constrained cable robots with elastic cables: variable stiffness formulation, in: Cable-Driven Parallel Robots, Springer, 2015, pp. 161–177.

[21] R. Babaghasabha, M. A. Khosravi, H. D. Taghirad, Adaptive robust control of fully-constrained cable driven parallel robots, Mechatronics 25 (2015) 27–36.

[22] X. Cui, W. Chen, G. Yang, Y. Jin, Closed-loop control for a cable-driven parallel manipulator with joint angle feedback, in: IEEE/ASME International Conference on Advanced Intelligent Mechatronics (AIM), 2013, IEEE, 2013, pp. 625–630.

[23] J.-J. E. Slotine, W. Li, et al., Applied nonlinear control, Vol. 199, Prentice hall Englewood Cliffs, NJ, 1991.

[24] B. Zhang, W. Shang, S. Cong, Dynamic control with tension compensation of a 3-dof cable-driven parallel manipulator, in: Cybernetics and Intelligent Systems (CIS) and IEEE Conference on Robotics, Automation and Mechatronics (RAM), 2017, IEEE, 2017, pp. 508–513.

[25] T. Bruckmann, W. Lalo, C. Sturm, D. Schramm, M. Hiller, Design and realization of a high rack storage and retrieval machine based on wire robot technology, in: International Symposium on Dynamic Problems of Mechanics. Proceedings, DINAME, 2013.

[26] S. Baklouti, S. Caro, E. Courteille, Elasto-dynamic model-based control of non-redundant cable-driven parallel robots, in: ROMANSY 22–Robot Design, Dynamics and Control, Springer, 2019, pp. 238–246.

[27] I. Ebert-Uphoff, P. A. Voglewede, On the connections between cable-driven robots, parallel manipulators and grasping, in: IEEE International Conference on Robotics and Automation, 2004. Proceedings. ICRA'04. 2004, Vol. 5, IEEE, 2004, pp. 4521–4526.

[28] A. Pott, An improved force distribution algorithm for over-constrained cable-driven parallel robots, in: Computational Kinematics, Springer, 2014, pp. 139–146.

[29] C. Gosselin, M. Grenier, On the determination of the force distribution in overconstrained cable-driven parallel mechanisms, Meccanica 46 (1) (2011) 3–15.

[30] P. H. Borgstrom, B. L. Jordan, G. S. Sukhatme, M. A. Batalin, W. J. Kaiser, Rapid computation of optimally safe tension distributions for parallel cable-driven robots, IEEE Transactions on Robotics 25 (6) (2009) 1271–1281.

[31] L. Mikelsons, T. Bruckmann, M. Hiller, D. Schramm, A real-time capable force calculation algorithm for redundant tendon-based parallel manipulators, in: IEEE International Conference on Robotics and Automation, 2008. ICRA 2008., IEEE, 2008, pp. 3869–3874.

[32] M. Arsenault, Workspace and stiffness analysis of a three-degree-of-freedom spatial cable-suspended parallel mechanism while considering cable mass, Mechanism and Machine Theory 66 (2013) 1–13.

[33] W. Khalil, E. Dombre, Modeling, identification and control of robots, Butterworth-Heinemann, 2004.

[34] S. Baklouti, S. Caro, E. Courteille, Sensitivity analysis of the elasto-geometrical model of cable-driven parallel robots, in: Cable-Driven Parallel Robots, Springer, 2018, pp. 37–49.

[35] A. Olabi, M. Damak, R. Bearee, O. Gibaru, S. Leleu, Improving the accuracy of industrial robots by offline compensation of joints errors, in: Industrial Technology (ICIT), 2012 IEEE International Conference on, IEEE, 2012, pp. 492–497.

[36] W. Verdonck, J. Swevers, Improving the dynamic accuracy of industrial robots by trajectory pre-compensation, in: Robotics and Automation, 2002. Proceedings. ICRA'02. IEEE International Conference on, Vol. 4, IEEE, 2002, pp. 3423–3428.

[37] S. Baklouti, E. Courteille, S. Caro, M. Dkhil, Dynamic and oscillatory motions of cable-driven parallel robots based on a non-linear cable tension model, Journal of Mechanisms and Robotics 9 (6) (2017) 061014.

[38] K. Kozak, Q. Zhou, J. Wang, Static analysis of cable-driven manipulators with non-negligible cable mass, IEEE Transactions on Robotics 22 (3) (2006) 425–433.